Pressure effect of the charge density wave transition on Raman spectra and transport properties of $2H$-$NbSe_2$

Zi-Yu Cao,[1] Kai Zhang,[1] Alexander F. Goncharov,[2] Xiao-Jun Yang,[3] Zhu-An Xu,[3] and Xiao-Jia Chen[4,*]

[1]*Center for High-Pressure Science & Technology Advanced Research, Beijing 100094, People's Republic of China*

[2]*Earth and Planets Laboratory, Carnegie Institution for Science, Washington, DC 20015, USA*

[3]*Department of Physics, Zhejiang University, Hangzhou 310027, China*

[4]*Department of Physics and Texas Center for Superconductivity, University of Houston, Houston, Texas 77204, USA*

(Received 14 March 2023; revised 10 May 2023; accepted 1 June 2023; published 15 June 2023)

Charge density wave (CDW) order is widely existing and fundamentally important in solid-state physics. However, several critical issues regarding the vibrational and electronic subsystems and their coupling still need to be better understood. Here, we tune the electrical transport and collective vibrational excitation, i.e., phonon and amplitude mode, by pressure in a prototype charge density wave material, $2H$-$NbSe_2$. A complete pressure-temperature phase diagram is revisited. The anomaly in Hall and magnetoresistivity at CDW critical temperature, T_{CDW}, was suppressed by the pressure. In the Raman spectroscopy measurements, the appearance of CDW amplitude mode is accompanied by the freezing of the two-phonon mode. The frequency of CDW amplitude mode under pressure follows modified mean-field theory with power-law scaling ($\beta = 0.18$). The renormalization of the Raman phonon across the CDW transition and the mean-field temperature dependence of CDW amplitude mode emphasized the importance of electron-phonon coupling in the formation of CDW state in $2H$-$NbSe_2$. Our work clarifies the complex vibrational and electronic subsystems and sheds light on the mechanism of the charge density state in $2H$-$NbSe_2$.

DOI: 10.1103/PhysRevB.107.245125

I. INTRODUCTION

The concept of a charge density wave (CDW) order originates from the Peierls transition of the electronic instabilities in one-dimensional metals as a consequence of Fermi-surface nesting, which suggests the real and imaginary parts of electronic susceptibility peak at a CDW wave vector due to Fermi-surface contours coincide when shifted along this wave vector [1,2]. As a result, the effective screening phonon by electron leads to zero energy in the phonon dispersion at the CDW wave vector, driving the periodic lattice distortion [3]. However, recent research evidence, especially in the two-dimensional or quasi-two-dimensional system, indicates that the nesting picture may help the CDW formation but cannot support the lattice distortion solely [4–6]. Instead, the q dependence of electron-phonon coupling may explain several key issues in forming the CDW state [4–6]. Besides the scenarios mentioned above, exciton-phonon interactions and saddle-point scenarios were also proposed and evidenced by several theory simulations and experiments [7–9]. Although extensive efforts have been made, the origin of CDW order in these compounds is still under debate [10–15].

Known for their quasi-two-dimensional character of the structure, transition-metal dichalcogenides (TMDs) are good candidates for the investigations of the CDW state. A layered quasi-two-dimensional TMD, $2H$-$NbSe_2$ is a prototypical CDW metal. The Se-Nb-Se bands are strongly covalent in a hexagonal polytype with two layers in the unit cell coupled by a weak van der Waals interaction [16]. The superconductivity was found in $2H$-$NbSe_2$ with the superconducting critical temperature (T_c) of 7.2 K [17]. After, an incommensurate nearly $3a \times 3a$ CDW order was discovered from neutron scattering at $T_{CDW} = 33.5$ K [18,19]. The lattice instability is also proved by the softening to zero energy (or imaginary frequency in theory) of the longitudinal acoustic (LA) phonon near CDW wave vector $q = 2/3\Gamma M$ [19,20]. From the high-pressure, low-temperature inelastic x-ray scattering measurements, this strong temperature dependence of the softening in LA phonon mode even persists up to 16 GPa, which is far above the pressure of collapse of the CDW state [21].

Raman spectroscopy is a powerful tool to detect the superconducting Higgs mode as well as layer-dependent CDW state in $2H$-$NbSe_2$ [22,23]. In the meantime, it provides an alternative way to investigate the phonon anomaly in high-pressure and low-temperature environments. One of the intense features in the Raman spectra of $2H$-$NbSe_2$ at ambient conditions is the broad two-phonon mode near 180 cm^{-1} [24], which originated from phonons with opposite momenta in the same acoustic branch [19,25]. It is demonstrated by the theory that the frequency of the two-phonon mode is approximately twice that of the soft LA phonon near $q = 2/3\Gamma M$ [26,27]. Thus, the capability of Raman spectroscopy is extended, at least in $2H$-$NbSe_2$, from probing zone-center phonons to vibrational excitations at the CDW wave vector. Moreover, the CDW collective excitations, known as amplitude mode, emerge in the Raman spectrum [28,29]. The high-pressure, low-temperature

*xjchen@uh.edu

Raman spectrum is expected to reveal how the CDW-driven force and order parameters change with temperature and pressure.

Here, we report electrical transport and Raman-scattering measurements of 2*H*-$NbSe_2$ at high pressures and low temperatures. We found that the kink in resistivity, change of sign of the Hall effect, and rapid increase of magnetoresistivity are indicators of the formation of the CDW state. These CDW-induced features in transport measurements can be strongly suppressed by the pressure. Meanwhile, the phonon mode, CDW driving force, CDW amplitude mode, and their evolution with temperature and pressure are well investigated by Raman spectroscopy.

II. EXPERIMENT METHODS

The standard iodine vapor transport method was used to grow the single crystals of 2*H*-$NbSe_2$. The crystal was grown using stoichiometric amounts of 99.9% pure Nb and 99.99% pure Se powders, together with a transport agent (iodine). The mixture was placed at the end of a quartz tube. The sealed quartz tube was heated in a temperature-gradient furnace with the charge-zone temperature of 1073 K and growth-zone temperatures of 998 K over three weeks. The quality of the single crystals was examined by x-ray-diffraction technique. A pair of ultralow-fluorescence standard-cut diamonds with a culet diameter of 400 μm was used in the experiment. The nonmagnetic 0.25-mm-thick rhenium was employed as a gasket and electrically insulated from the electrodes by a mixture of epoxy and c-BN. A sample chamber of diameter 150 μm was formed by laser drilling in the center of c-BN. The single-crystal 2*H*-$NbSe_2$ was exfoliated to the thickness of around 5 μm and cut to a regular shape by the blade. Four Pt wires with a thickness of 3–4 μm were adhered to a $90 \times 90 \times 5\mu m^3$ high-quality single-crystal 2*H*-$NbSe_2$ with silver epoxy by van der Pauw configuration. Daphne oil 7373 and neon was used as the pressure-transmitting medium to ensure hydrostatic pressure conditions for the transport and Raman measurement, respectively. The pressure was calibrated by the spectral shift of the fluorescence R1 peak of ruby right after the measurement was down. The electrical transport properties were measured in a Physical Property Measurement System by Quantum Design. A He4 continuous-flow cryostat was used as a refrigerator for low-temperature Raman measurement. The Raman-scattering measurements were measured by the laser excitation wavelengths of 488 nm, which were delivered by a narrow-line solid-state laser. A custom-made microscope with a Mitutoyo 20× long working-distance objective lens collects the Raman signal in a backscattering geometry. The Raman spectra were measured using a single-stage spectrograph equipped with a thermoelectrically cooled charge-coupled device detector with laser power down to 0.2 mW to avoid laser heating effects.

III. RESULTS AND DISCUSSION

Although 2*H*-$NbSe_2$ is a well-investigated compound, we revisited the pressure-temperature phase diagram based on the electrical transport and Raman measurement, shown in Fig. 1. Daphne oil 7373 was used as the pressure-transmitting medium in all the electrical transport measurements. Neon was used for the low-temperature Raman measurement. According to the previous investigation on the hydrostatic limit of the pressure medium [30], the hydrostatic pressure of Daphne oil and neon can be maintained up to 3.7 and 15 GPa, respectively. The T_{CDW} detected from these two measurements show a good agreement with each other, indicating a hydrostatic environment in the measurement of the CDW state. Figure 2(a) displays the temperature dependence of electrical resistivity, $R(T)$, at various pressures. The CDW gap opens, evidenced by the appearance of a hump in $R(T)$ at 33.5 K, below which resistivity demonstrates metallic behavior. The unimpressive hump indicates that only a tiny portion of the Fermi surface is gapped, which is supported by an angle-resolved photoemission spectroscopy study [31]. As the pressure increases, the T_{CDW} is monotonically suppressed as a CDW state collapses at the pressure of 3.7 GPa. In the pressure range, where T_{CDW} drops fast, the T_c is enhanced steeply. Above 3.7 GPa, the T_c increases steadily to the T_c maximum of 9.4 K at the pressure of 17.8 GPa, followed by a gradual decrease of T_c. It is worth noting that the superconducting dome maximum is avoided at the CDW collapse pressure, which indicates that the superconductivity is not induced by CDW quantum fluctuation. The T_c is reduced inside the CDW phase simply because of the loss of density of states [32].

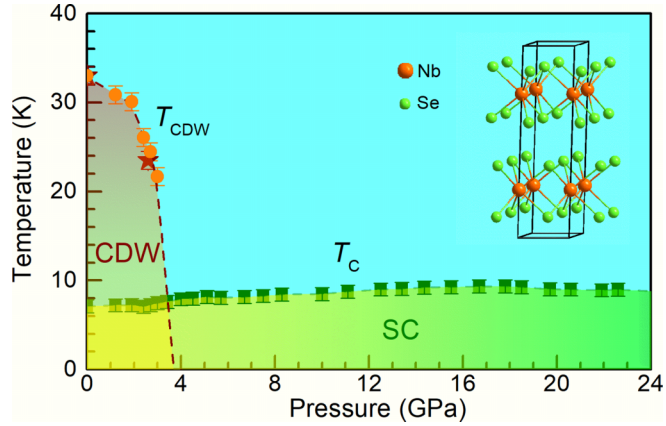

FIG. 1. Pressure-temperature phase diagram of 2*H*-$NbSe_2$ from resistivity (orange dot and green square) and Raman spectrum (red star). Inset is the crystallographic structure of 2*H*-$NbSe_2$. T_c maximum is 9.4 K at 17.8 GPa.

Figures 2(b) and 2(c) display the temperature dependence of the electrical Hall coefficient and magnetoresistivity, respectively. The Hall effect and magnetoresistivity exhibit distinct features near the CDW transition. The Hall coefficient suddenly drops at around 34 K and changes its sign at a lower temperature of 28 K. Additionally, magnetoresistivity grows significantly below T_{CDW}. These CDW-induced features can be strongly suppressed by the pressure. It has been widely reported that the sign of the Hall coefficient changes near T_{CDW} [32,33], described by several scenarios such as being driven by pseudogap opening [34] or sharp changes of the scattering rate on electron-like orbit in the framework of a two-band model [35]. The magnetoresistivity in 2*H* -$NbSe_2$, although only 30% at 10 K and 9 T, is nearly linear and

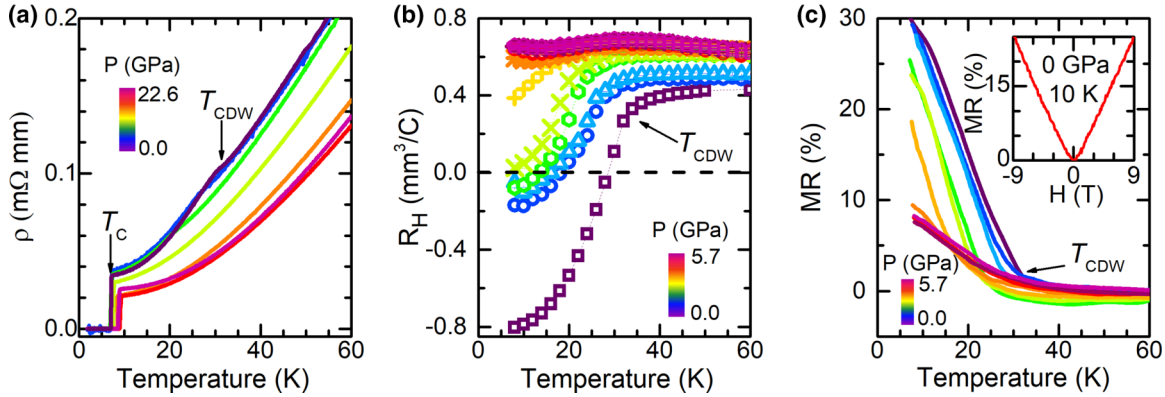

FIG. 2. (a) Temperature dependence of electrical resistivity at high pressures (1 bar–22.6 GPa). Hump in the resistivity around temperature of 33.5 K indicates appearance of the CDW state. T_c is around 7.2 K. (b) Temperature dependence of Hall coefficient under pressure. For clear observation of sign change of Hall coefficient, zero Hall coefficient is marked as a dashed line. (c) Magnetoresistivity [$MR = \frac{\rho(9T)-\rho(0T)}{\rho(0T)} \times 100\%$)] as a function of temperature under pressure. Inset of (c) shows field dependence of unsaturated MR at ambient pressure and 10 K.

unsaturated, which departs from the behavior in the normal metal. Such a small magnetoresistivity rules out the possibility of perfect electron-hole compensation, which is discovered in TMD compound WTe_2, owing to 452 700% at 4.5 K in a field of 14.7 T [36]. Instead, the orbit magnetoresistivity, such as weakly open orbits generated by folded superstructure in CDW state, is consistent with our observation. Meanwhile, the open-orbit reversal of the local curvature of the Fermi surface may lead to an electron-like Hall effect even though the Fermi surface cross section has a global holelike topology [37]. The driving mechanism of the abnormal electric transport nature in $2H$-$NbSe_2$ still merits further study.

Raman spectroscopy is an effective tool to probe the vibrational and CDW excitations. We applied this technique at high pressures and low temperatures to investigate the CDW mechanism. Figure 3 represents the intensity contour plot in the Raman shift–temperature plane. The spectra were normalized by the Bose factor for Stokes side by $I(\omega) = I_0(\omega)/[N(\omega, T) + 1]$, where $N(\omega, T)$ is the Bose-Einstein distribution function. At ambient pressure, $2H$-$NbSe_2$ has a crystal structure of hexagonal D^4_{6h} symmetry [16]. The structural motif consists of a trigonal prism of Se atoms surrounded by a Nb atom. Based on the lattice symmetry, the Raman-active phonon branch includes E^2_{2g}, A_{1g}, E_{1g}, and E^1_{2g}. The E_{1g} phonon, due to the insignificant scattering cross section, is undetectable. In addition, a two-phonon mode is observed in the Raman spectra at temperatures above 50 K. Below T_{CDW}, the CDW amplitude mode is present.

The spectra are fitted by means of the damped harmonic oscillator (for low frequencies and amplitude mode) combination of the Lorentzian line shapes (for phonon mode). The pressure and temperature evolution of the frequency of phonon modes of $2H$-$NbSe_2$ is shown in Fig. 4. At pressure below 3.7 GPa [Figs. 4(a) and 4(b)], all the phonon modes E^2_{2g}, A_{1g}, and E^1_{2g} exhibit blueshifts with decreasing temperature above T_{CDW}. However, below T_{CDW}, the

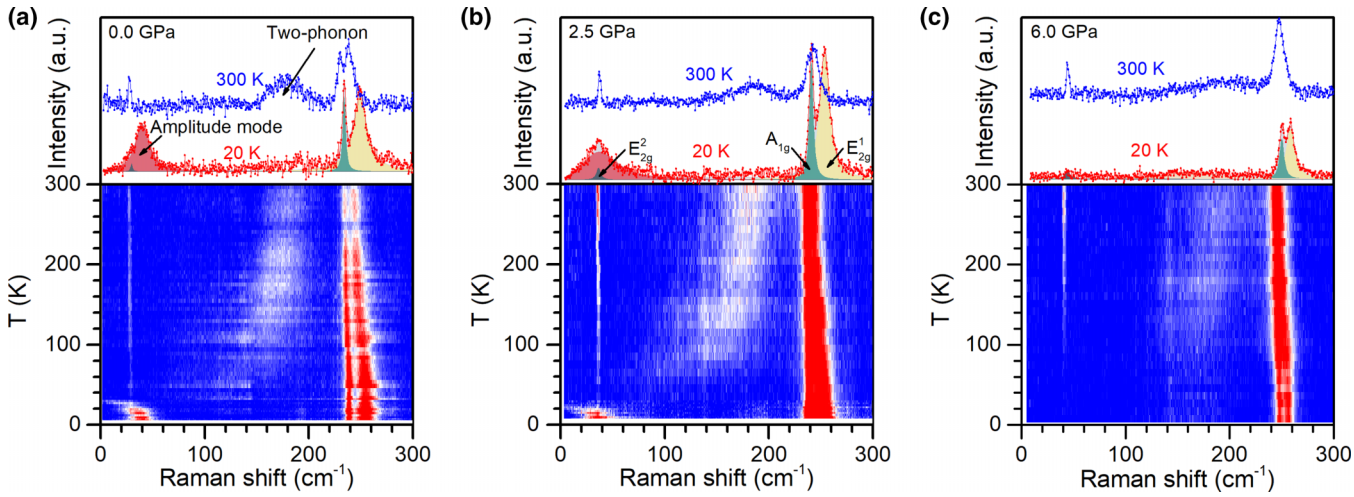

FIG. 3. (a)–(c) Raman data of $2H$ -$NbSe_2$ at various temperatures at 0 GPa (a), 2.5 GPa (b), and 6.0 GPa (c). Upper panels are spectra at typical temperatures. Raman-active mode A_{1g}, E_{1g}, $\mathbf{E^1_{2g}}$, and $\mathbf{E^2_{2g}}$ are marked, respectively. Two-phonon mode at high temperatures and CDW amplitude mode below T_{CDW} can also be observed. Contour map of Raman intensity is plotted in Raman shift–temperature plane in the bottom panel. Same intensity scale was used in the 2D presentation for a better comparison.

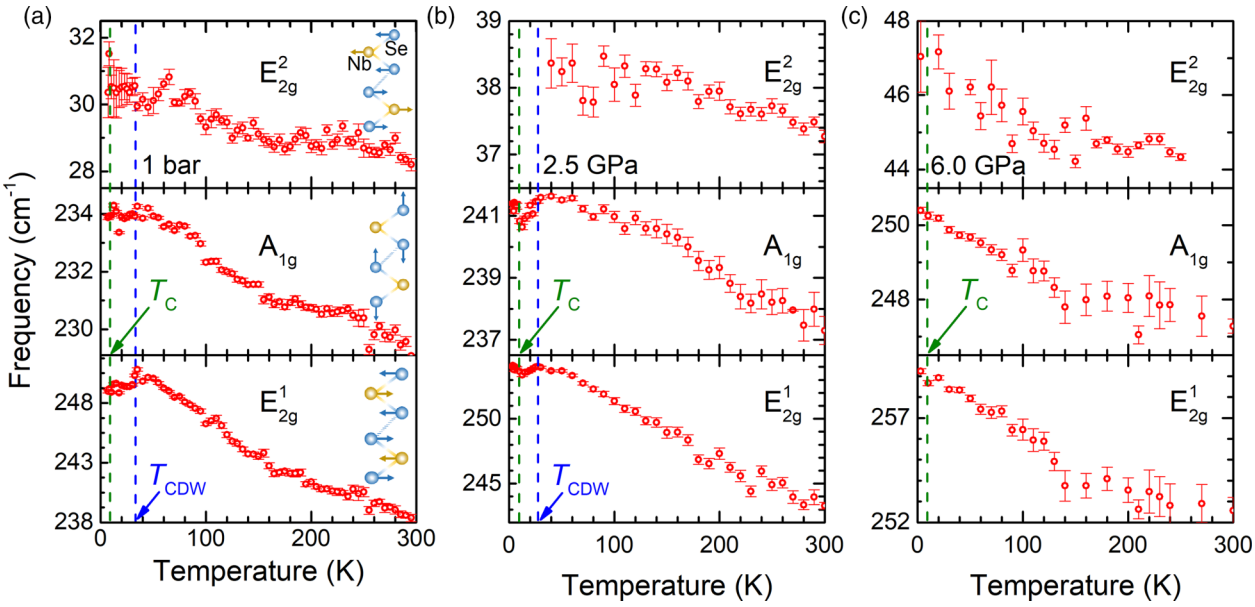

FIG. 4. (a) Frequency of Raman-active mode as a function of temperature at ambient pressure. Insets are vibrational modes for each phonon. (b) Temperature dependence of phonon frequency at 2.5 GPa. Due to overlap of $\mathbf{E}^2_{2g}$ mode and CDW amplitude mode, frequency of $\mathbf{E}^2_{2g}$ is undistinguishable at low temperatures. (c) Temperature dependence of phonon frequency at 6.0 GPa where CDW is collapsed. Blue and olive dashed lines represents CDW and superconducting transition temperature in phase diagram.

phonon frequency trends change across the CDW transition. The frequencies of E^1_{2g} and A_{1g} modes are nearly temperature independent at low temperature and even tend to decrease upon cooling. The CDW distortion affects both the in-plane and out-of-plane vibration, which is similar to previous reports on other TMDs [13,15]. At temperature near T_c, the frequencies of these phonons upturn again, especially at 2.5 GPa. When the pressure increases to 6 GPa, the frequencies of phonon modes exhibit monotonous hardening with cooling. Clearly, the periodic modulation of the charge density is coupled with superlattice phonon mode, providing evidence of sizable electron-phonon coupling in 2H-$NbSe_2$.

The understanding of softening of acoustic phonon is one of the key points to understanding the CDW mechanism in 2H-$NbSe_2$ [38]. As we mentioned above, the theory predicts that the frequency of the two-phonon mode is approximately twice of the soft LA phonon at $q = 2/3\Gamma M$ [26,27]. Figure 5 displays the peak position and linewidth of the two-phonon and CDW amplitude mode at the pressure points of interest of the CDW state at low temperatures. Based on the phase diagram in Fig. 1, the CDW state holds at 0 and 2.5 GPa but is absent at 6.0 GPa. Upon cooling from room temperature to T_{CDW}, the intensity of the two-phonon mode becomes weaker and shows a long-range softening from 181 to 115 cm^{-1} at

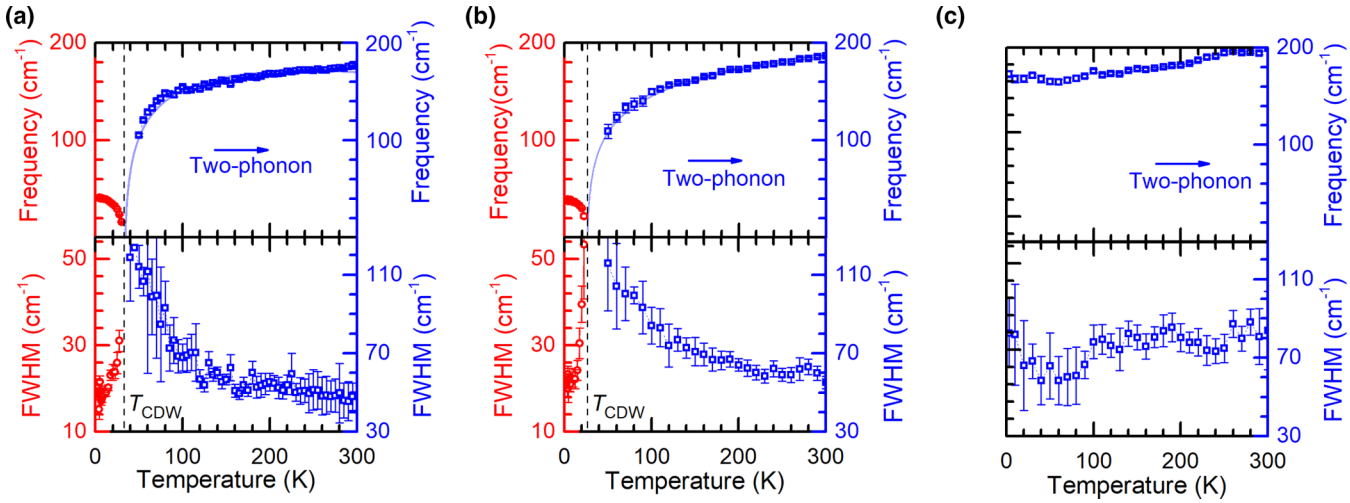

FIG. 5. (a)–(c) Two-phonon and CDW amplitude modes of 2H -$NbSe_2$ at 0 GPa (a), 2.5 GPa (b), and 6.0 GPa (c). Upper and lower panels show how mode frequency and full width at half maximum vary with temperature. T_{CDW} below CDW collapsed pressure is marked as a dashed line.

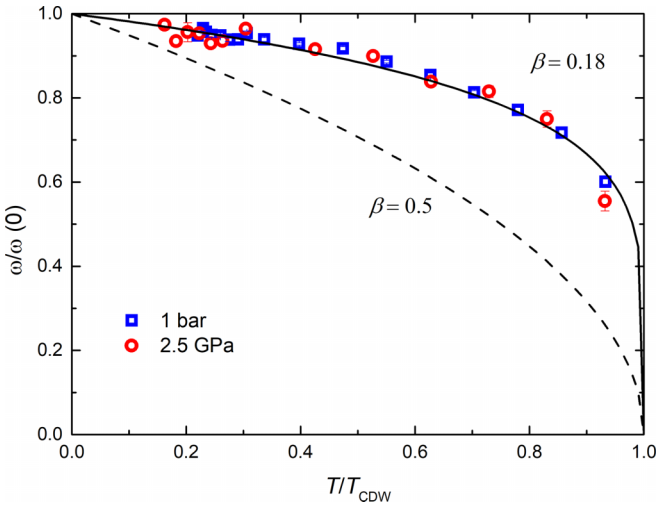

FIG. 6. Reduced frequency of amplitude mode vs reduced temperature. Blue squares and red dots are CDW amplitude mode at ambient pressure and 2.5 GPa, respectively. Black line corresponds to a fit using a modified mean-field calculation $\omega(T)/\omega(0) \sim (1-T/T_{\mathrm{CDW}})^{\beta}$ with $\beta = 0.18$. Classical mean-field calculation with $\beta = 0.5$ is shown as a dashed line for comparison.

ambient pressure and 187 to 125 cm^{-1} at 2.5 GPa. Although the two-phonon mode vanishes at a temperature slightly above T_{CDW}, the frequency trend decreases and extrapolates to zero frequency at T_{CDW}. Meanwhile, the full width at half maximum of the two-phonon mode increases remarkably, which can be accounted for by strong anharmonic interaction upon cooling [27]. Once the temperature is below T_{CDW}, the CDW amplitude mode appears, gains intensity, hardens, and sharpens. Our data at different pressures (Fig. 3) show that this behavior becomes less prominent with pressure until the CDW state collapses above 3.7 GPa. When pressure is increased to 6 GPa, the two-phonon mode exhibits a limited softening from 194 to 173 cm^{-1} and it can be observed down to 3 K. This behavior indicates that CDW is suppressed under these conditions. Moreover, at 6 GPa, the full width at half maximum is nearly temperature independent, indicating that the anharmonic interaction seems inconspicuous above CDW collapsed pressure.

The CDW collective mode associated with the broken symmetry is linked to the CDW order parameter. Therefore, it is expected to have a mean-field-like temperature dependence, $\omega(T) = 1.4\Lambda^{1/2}\tilde{\omega}(1-t)^{\beta}$ [24], where the $\tilde{\omega}$ is the unscreened, or high-temperature phonon frequency, t is the reduced temperature T/T_{CDW}, $\beta = 0.5$, and Λ is the electron-phonon coupling constant associated with CDW. However, this expectation fails to describe what we observed. Instead, a relaxation of the fitting parameter β of 0.18 may provide an excellent fit. The departure from the square-root dependence of CDW amplitude mode has also been shown in other TMDs or doped TMDs [39,40]. For a universal analysis, the reduced temperature dependence of the reduced frequency of amplitude mode under pressure is shown in Fig. 6. Interestingly, all the datasets of amplitude mode collapse onto the same curve given by $\omega(T)/\omega(0) = (1-t)^{0.18}$, where $\omega(0)$ is the CDW amplitude mode frequency at 0 K, suggesting that the external hydrostatic pressure does not affect the mechanism of CDW formation. The increase in pressure hardens the unscreened phonon frequency $\tilde{\omega}$. $(1-t)^{\beta}$ does not have a significant pressure dependence. The decrease of amplitude mode energy $\omega(T)$ with pressure suggests the suppression of CDW is associated with a substantial reduction in the electron-phonon coupling constant Λ at the CDW wave vector. $\Lambda = Ng^2(q)$, where N is the joint density of states of the electrons or holes involved in the CDW translation. $g(q)$ is the q-dependent electron-phonon coupling matrix element. If $g(q_{\mathrm{CDW}})$ decreases remarkably with pressure in a system with weak Fermi-surface nesting, such as in $2H$-$NbSe_2$ [5], the imaginary phonon will vanish at CDW wave vector due to the decrease of screening energy, $|g(q)|^2\mathrm{Re}[\chi(q,\omega)]$, where $\mathrm{Re}[\chi(q,\omega)]$ is the real part of susceptibility. In this case, the electron-phonon coupling plays an essential role in the formation of the CDW state.

IV. CONCLUSIONS

In conclusion, we have reported the electrical transport and Raman-scattering measurements of $2H$-$NbSe_2$ at high pressures and low temperatures. All the CDW-induced features in transport measurements can be strongly suppressed by the pressure. The open orbits generated by folded superstructure in CDW state are appropriate to explain our observation of the change of sign of the Hall effect and rapid increase of magnetoresistivity. In the high-pressure, low-temperature Raman-scattering measurements, the appearance of CDW amplitude mode is accompanied by the freezing of the two-phonon mode. We found that the charge density wave transition is strongly hybridized with other Raman active phonons, e.g., A_{1g} and E^1_{2g} mode, suggesting the strong electron-phonon coupling in $2H$-$NbSe_2$, which is also supported by the pressure and temperature evolution of amplitude mode in modified mean-field theory. This demonstrates a clear connection between the vibrational and electronic subsystems of $2H$-$NbSe_2$, which our investigation revealed by tuning the pressure.

ACKNOWLEDGMENTS

The work at ZJU was supported by National Natural Science Foundation of China (No. 12174334).

[1] G. Grüner, The dynamics of charge-density waves, Rev. Mod. Phys. **60**, 1129 (1988).

[2] M. H. Whangbo, E. Canadell, P. Foury, and J. P. Pouget, Hidden Fermi surface nesting and charge density wave instability in low-dimensional metals, Science **252**, 96 (1991).

[3] W. Kohn, Image of the Fermi Surface in the Vibration Spectrum of a Metal, Phys. Rev. Lett. **2**, 393 (1959).

[4] D. W. Shen, B. P. Xie, J. F. Zhao, L. X. Yang, L. Fang, J. Shi, R. H. He, D. H. Liu, H. H. Wen, and D. L. Feng, Novel Mechanism of a Charge Density Wave in a Transition Metal Dichalcogenide, Phys. Rev. Lett. **99**, 216404 (2007).

[5] X. Zhu, Y. Cao, J. Zhang, E. W. Plummer, and J. Guo, Classification of charge density waves based on their nature, Proc. Natl. Acad. Sci. USA **112**, 2367 (2015).

[6] T. Valla, A. V. Fedorov, P. D. Johnson, P-A. Glans, C. McGuinness, K. E. Smith, E. Y. Andrei, and H. Berger, Quasiparticle Spectra, Charge-Density Waves, Superconductivity, and Electron-Phonon Coupling in 2*H* -$NbSe_2$, Phys. Rev. Lett. **92**, 086401 (2004).

[7] T. M. Rice and G. K. Scott, New Mechanism for a Charge-Density-Wave Instability, Phys. Rev. Lett. **35**, 120 (1975).

[8] C. Monney, C. Battaglia, H. Cercellier, P. Aebi, and H. Beck, Exciton Condensation Driving the Periodic Lattice Distortion of 1*T* -$TiSe_2$, Phys. Rev. Lett. **106**, 106404 (2011).

[9] R. Liu, C. G. Olson, W. C. Tonjes, and R. F. Frindt, Momentum Dependent Spectral Changes Induced by the Charge Density Wave in 2*H* -$TaSe_2$ and the Implication on the CDW Mechanism, Phys. Rev. Lett. **80**, 5762 (1998).

[10] M. D. Johannes, I. I. Mazin, and C. A. Howells, Fermi-surface nesting and the origin of the charge-density wave in $NbSe_2$, Phys. Rev. B **73**, 205102 (2006).

[11] G. Liu, X. Ma, K. He, Q. Li, H. Tan, Y. Liu, J. Xu, W. Tang, K. Watanabe, T. Taniguchi, L. Gao, Y. Dai, H. Wen, B. Yan, and X. Xi, Observation of anomalous amplitude modes in the kagome metal CsV_3Sb_5, Nat. Commun. **13**, 3461 (2022).

[12] T. Wu, H. Mayaffre, S. Krämer, M. Horvatić, C. Berthier, W. N. Hardy, R. Liang, D. A. Bonn, and M. Julien, Magnetic-field-induced charge-stripe order in the high-temperature superconductor $YBa_2Cu_3O_y$, Nature (London) **477**, 191 (2011).

[13] X. Zhao, K. Zhang, Z. Cao, Z. Zhao, V. V. Struzhkin, A. F. Goncharov, H. Wang, A. G. Gavriliuk, H. Mao, and Xiao-Jia Chen, Pressure tuning of the charge density wave and superconductivity in 2*H* -TaS_2, Phys. Rev. B **101**, 134506 (2020).

[14] K. Zhang, H. Jiang, J. Yang, J. Zhang, Z. Zeng, X. Chen, and F. Su, Pressure effects on the lattice vibrations and ultrafast photocarrier dynamics in 2*H* -TaS_2, Appl. Phys. Lett. **117**, 101105 (2020).

[15] K. Zhang, Z. Y. Cao, and X. J. Chen, Effects of charge-density-wave phase transition on electrical transport and Raman spectra in 2*H* -tantalum disulfide, Appl. Phys. Lett. **114**, 141901 (2019).

[16] G. P. Chen, E. Bykova, M. Bykov, E. Edmund, Z. Cao, X. Chen, J. S. Smith, S. Chariton, V. B. Prakapenka, and A. F. Goncharov, Structural and vibrational behavior of 2*H* -$NbSe_2$ at high pressures, Phys. Rev. B **105**, 224114 (2022).

[17] E. Revolinsky, G. A. Spiering, and D. J. Beerntsen, Superconductivity in the niobium-selenium system, J. Phys. Chem. Solids **26**, 1029 (1965).

[18] J. A. Wilson, F. J. D. Salvo, and S. Mahajan, Charge-density waves and superlattices in the metallic layered transition metal dichalcogenides, Adv. Phys. **50**, 1171 (2001).

[19] D. E. Moncton, J. D. Axe, and F. J. Disalvo, Study of Superlattice Formation in 2*H* -$NbSe_2$ and 2*H* -$TaSe_2$ by Neutron Scattering, Phys. Rev. Lett. **34**, 734 (1975).

[20] F. Weber, R. Hott, R. Heid, K.-P. Bohnen, S. Rosenkranz, J.-P. Castellan, R. Osborn, A. H. Said, B. M. Leu, and D. Reznik, Optical phonons and the soft mode in 2*H* -$NbSe_2$, Phys. Rev. B **87**, 245111 (2013).

[21] M. Leroux, I. Errea, M. L. Tacon, S.-M. Souliou, G. Garbarino, L. Cario, A. Bosak, F. Mauri, M. Calandra, and P. Rodière, Strong anharmonicity induces quantum melting of charge density wave in 2*H* -$NbSe_2$ under pressure, Phys. Rev. B **92**, 140303(R) (2015).

[22] X. Xi, L. Zhao, Z. Wang, H. Berger, L. Forró, J. Shan, and K. Mak, Strongly enhanced charge-density-wave order in monolayer $NbSe_2$, Nat. Nanotechnol. **10**, 765 (2015).

[23] R. Grasset, T. Cea, Y. Gallais, M. Cazayous, A. Sacuto, L. Cario, L. Benfatto, and M. Méasson, Higgs-mode radiance and charge-density-wave order in 2*H* -$NbSe_2$, Phys. Rev. B **97**, 094502 (2018).

[24] J. C. Tsang, J. E. Smith, and M. W. Shafer, Raman Spectroscopy of Soft Modes at the Charge-Density-Wave Phase Transition in 2*H* -$NbSe_2$, Phys. Rev. Lett. **37**, 1407 (1976).

[25] Y. Wu, M. An, R. Xiong, J. Shi, and Q. M. Zhang, Raman scattering spectra in the normal phase of 2*H* -$NbSe_2$, J. Phys. D: Appl. Phys. **41**, 175408 (2008).

[26] M. V. Klein, Theory of two-phonon Raman scattering in transition metals and compounds, Phys. Rev. B **24**, 4208 (1981).

[27] S. N. Behera and G. C. Mohanty, Theory of two-phonon modes in layered charge-density-wave systems, Pramana - J. Phys. **26**, 239 (1986).

[28] M. Rice and S. Strässler, Theory of the soft phonon mode and dielectric constant below the Peierls transition temperature, Solid State Commun. **13**, 1931 (1973).

[29] S. Sugai, Lattice vibrations in the charge-density-wave states of layered transition metal dichalcogenides, Phys. Status Solidi B **129**, 13 (1985).

[30] S. Klotz, J. C. Chervin, P. Munsch, and G. L. Marchand, Hydrostatic limits of 11 pressure transmitting media, J. Phys. D: Appl. Phys. **42**, 075413 (2009).

[31] D. J. Rahn, S. Hellmann, M. Kalläne, C. Sohrt, T. K. Kim, L. Kipp, and K. Rossnagel, Gaps and kinks in the electronic structure of the superconductor 2*H* -$NbSe_2$ from angle-resolved photoemission at 1 K, Phys. Rev. B **85**, 224532 (2012).

[32] O. Moulding, I. Osmond, F. Flicker, T. Muramatsu, and S. Friedemann, Absence of superconducting dome at the charge-density-wave quantum phase transition in 2*H* -$NbSe_2$, Phys. Rev. Res. **2**, 043392 (2020).

[33] H. N. S. Lee, H. McKinzie, D. S. Tannhauser, and A. Wold, The low-temperature transport properties of $NbSe_2$, J. Appl. Phys. **40**, 602 (1969).

[34] D. V. Evtushinsky, A. A. Kordyuk, V. B. Zabolotnyy, D. S. Inosov, B. Büchner, H. Berger, L. Patthey, R. Follath, and S. V. Borisenko, Pseudogap-Driven Sign Reversal of the Hall Effect, Phys. Rev. Lett. **100**, 236402 (2008).

[35] L. J. Li, Z. A. Xu, J. Q. Shen, L. M. Qiu, and Z. H. Gan, The effect of a charge-density wave transition on the transport properties of 2*H* -$NbSe_2$, J. Phys.: Condens. Matter **17**, 493 (2005).

[36] M. N. Ali, J. Xiong, S. Flynn, J. Tao, Q. D. Gibson, L. M. Schoop, T. Liang, N. Haldolaarachchige, M. Hirschberger, N. P. Ong, and J. R. Cava, Large, non-saturating magnetoresistance in WTe_2, Nature (London) **514**, 205 (2014).

[37] N. P. Ong, Geometric interpretation of the weak-field Hall conductivity in two-dimensional metals with arbitrary Fermi surface, Phys. Rev. B **43**, 193 (1991).

[38] F. Weber, S. Rosenkranz, J.-P. Castellan, R. Osborn, R. Hott, R. Heid, K.-P. Bohnen, T. Egami, A. H. Said, and D. Reznik, Extended Phonon Collapse and the Origin of the Charge-Density Wave in $2H$-$NbSe_2$, Phys. Rev. Lett. **107**, 107403 (2011).

[39] J. Joshi, H. M. Hill, S. Chowdhury, C. D. Malliakas, F. Tavazza, U. Chatterjee, A. R. H. Walker, and P. M. Vora, Short-range charge density wave order in $2H$-TaS_2, Phys. Rev. B **99**, 245144 (2019).

[40] H. Barath, M. Kim, J. F. Karpus, S. L. Cooper, P. Abbamonte, E. Fradkin, E. Morosan, and R. J. Cava, Quantum and Classical Mode Softening Near the Charge-Density-Wave–Superconductor Transition of Cu_xTiSe_2, Phys. Rev. Lett. **100**, 106402 (2008).